IN-39

22329

21 P

NASA Technical Memorandum 106631

The Role of Crack Formation in Chevron-Notched Four-Point Bend Specimens

Anthony M. Calomino
Lewis Research Center
Cleveland, Ohio

and

Louis J. Ghosn
Case Western Reserve University
Cleveland, Ohio

August 1994

National Aeronautics and
Space Administration

THE ROLE OF CRACK FORMATION IN CHEVRON-NOTCHED FOUR-POINT BEND SPECIMENS

Anthony M. Calomino
National Aeronautics and Space Administration
Lewis Research Center
Cleveland, Ohio 44135

and

Louis J. Ghosn[*]
Case Western Reserve University
Cleveland, Ohio 44106

SUMMARY

The failure sequence following crack formation in a chevron-notched four-point bend specimen is examined in a parametric study using the Bluhm slice synthesis model. Premature failure resulting from crack formation forces which exceed those required to propagate a crack beyond α_{min} is examined together with the critical crack length and critical crack front length. An energy based approach is used to establish factors which forecast the tendency of such premature failure due to 0 crack formation for any selected chevron-notched geometry. A comparative study reveals that, for constant values of α_1 and α_0, the dimensionless beam compliance and stress intensity factor are essentially independent of specimen width and thickness. The chevron tip position, α_0, has its primary effect on the force required to initiate a sharp crack. Small values for α_0 maximize the stable region length, however, the premature failure tendency is also high for smaller α_0 values. Improvements in premature failure resistance can be realized for larger values of α_0 with only a minor reduction in the stable region length. The stable region length is also maximized for larger chevron base positions, α_1, but the chance for premature failure is also raised. Smaller base positions improve the premature failure resistance with only minor decreases in the stable region length. Chevron geometries having a good balance of premature failure resistance, stable region length, and crack front length are $0.20 \le \alpha_0 \le 0.30$ and $0.70 \le \alpha_1 \le 0.80$.

---

[*]NASA Resident Research Associate at Lewis Research Center.

a	crack length
A	Chevron crack area
$\alpha = \dfrac{a}{W}$	dimensionless crack length
$\alpha_0 = a_0/W$	dimensionless tip position of the chevron ligament
$\alpha_1 = a_1/W$	dimensionless base position of the chevron ligament
α_{min}	dimensionless crack length at $dG(\alpha)/d\alpha = 0$
B	thickness of the bend beam
$\beta_{min} = \dfrac{\alpha_{min} - \alpha_0}{\alpha_1 - \alpha_0}$	dimensionless crack width at $dG(\alpha)/d\alpha = 0$
$C_S(\alpha)$	dimensionless straight-through crack specimen compliance, $(\delta E'B)/P$
$C_V(\alpha)$	dimensionless chevron-notched specimen compliance, $(\delta E'B)/P$
$\Delta\alpha_{min} = \alpha_{min} - \alpha_0$	dimensionless subcritical region length increment
δ	load-line displacement
$\Delta\alpha = \alpha - \alpha_0$	dimensionless crack growth increment
E'	plane stress, $E = E'$, plane strain, $E' = E/(1 - v^2)$, elastic modulus
$G(\alpha)$	elastic energy release rate
G_{IC}	critical elastic energy release rate
k	shear correction term for Bluhm slice model
$K_I(\alpha)$	Mode I stress intensity factor
K_{IC}	critical Mode I stress intensity factor
n	number of slices through cross section for Bluhm model
v	Poisson's ratio
$\Delta\Omega$	fracture energy exhausted after crack formation and arrest

P	force applied to beam at the load-line
ρ	notch radius at chevron tip
S_1	load span distance
S_2	support span distance
S_P	fixed-force overload resistance factor
S_D	fixed-displacement overload resistance factor
σ_{cr}	critical stress for crack formation at chevron tip position
θ	base angle of chevron cross-section
ΔU	change in strain energy after crack formation and arrest
W	width of bend specimen
$Y_S(\alpha)$	dimensionless stress intensity for straight-through cracked beam
$Y_V(\alpha)$	dimensionless stress intensity for chevron-notched cracked beam
$z = \dfrac{B}{n}$	slice thickness for the Bluhm model

INTRODUCTION

The chevron-notched four-point bend specimen provides a convenient method for measuring the fracture resistance of very brittle materials which are difficult to precrack. The appeal of this specimen is its ability to form a sharp precrack from the machined notch without cyclic loading. By virtue of its geometry, the chevron notch geometry forms a crack during the early portion and that crack arrests immediately its formation. During the first stages of the crack's advance fracture energy requirements exceed elastic supply rates resulting in reduced fracture energy release rates. However, because the machined notch is blunt initiating a sharp crack often requires overloading. If the force required to form a sharp crack exceeds that required to propagate it through the specimen, the advantage of the chevron notch is lost. Understanding how a selected chevron geometry controls crack formation and subsequent crack advance is vital to the design of a standard chevron-notch test specimen configuration.

This paper presents a comprehensive examination of the effects a chevron geometry has on the stable region length, the included fracture area, and the tendency for premature failure for the four-point bend specimen. The resistance to premature failure is characterized by an overload resistance factor formulated to measure the resistance available to arrest a sharp crack after formation from an overload. A comparative parametric study is conducted using the Bluhm slice model (ref. 1)

3

approximations for beam compliance. This work establishes parameters which can aid in the selection of a four-point bend chevron geometry for standard fracture resistance measurements.

CRACK FORMATION STABILITY AND OVERLOAD RESISTANCE FACTOR

The schematic of a chevron-notched four-point bend specimen in figure 1 gives the geometric dimensions which influence its fracture performance. It is the trapezoidal shape of the uncracked ligament which produces stability during the early stages of crack growth. The fracture area, and therefore the fracture resistance, increases quadratically with increasing crack length. Correspondingly, beam compliance increases are less than quadratic which produces the negative sloped energy release rate curve shown in figure 2. This portion of the curve is referred to as the stable region of crack growth. The stable behavior is lost as the crack extends past the critical point, defined by $\Delta\alpha_{min}$ in figure 2, where the elastic energy supply rate and fracture energy requirements are equal. The energy release rate curve reaches a minimum and instability results for any additional loading since stable extension can no longer accommodate the potential release of elastic energy. Fracture stability is controlled by such geometric factors as the dimensionless tip and base positions of the chevron, $\alpha_0=a_0/W$ and $\alpha_1=a_1/W$, the width and thickness of the beam, W and B, and the support and loading spans, S_1 and S_2.

Once a geometry is selected, the energy release rate function, $G_I(\alpha)$, the stress intensity function,[1] $K_I(\alpha)$, the critical position, $\alpha_{min}=a_{min}/W$, the corresponding critical crack length increment, $\Delta\alpha_{min}=\alpha_{min}-\alpha_0$, and critical crack front length, $\beta_{min}=(\alpha_{min}-\alpha_0)/(\alpha_1-\alpha_0)$, are determined from a simple solution for the bend specimen compliance. The concept of overload failure due to bluntness of a machined notch was first considered in detail by Bluhm (ref. 2) when he analyzed stability in the 'work of fracture' (WOF) specimen. His objective was to develop a geometry having a stable region which extended through the full uncracked ligament of the beam. Bluhm recognized that the slope of the stress intensity function, $dK_I(\alpha)/d\alpha$, would influence the overload failure. He surmised that maximizing the negative slope of the stable region would optimize the overload failure resistance. He proposed factors which could be used to evaluate this resistance for any four-point bend chevron-notched geometry. Wu (ref. 8) later employed Bluhm's formulation to characterize the overload failure of chevron-notched three-point bend specimens. Wu concluded that Bluhm's approach, when applied to the three-point bend beam, resulted in conflicting design trends which he could not fully resolve.

The inconsistencies noted by Wu are resolved if other features relating to chevron-notching beside $dK_I(\alpha)/d(\alpha)$ are included when assessing crack formation stability. Although Bluhm's approach includes the difference in energy supply rate between selected geometries, no account is made for notch acuity and crack arrest capacity before instability. These features can be included by comparing the excess elastic energy available to sustain propagation after formation and the resistance energy available to arrest the crack before instability[2]. An overload resistance factor then can be evaluated as the ratio of the resistance energy to the driving energy. With this definition, chevron geometries having high overload resistance factors are less susceptible to premature failure at crack formation.

---

[1] A linear elastic fracture mechanics treatment is assumed such that $G_I(\alpha)=K_I^2(\alpha)/E$.

[2] Although an energy formulation is used to develop the overload resistance factor, a force balance method where $K_{IC}>K_I(\alpha<\alpha_{min})$ produces similar results.

4

The physical basis for the approach is that arrest will occur if the driving energy is less than the resistance energy. Larger resistive energy in comparison to driving energy improves the chance for crack arrest.

The driving energy for crack advance is the change in elastic energy from formation to crack arrest which is formulated for both a constant applied force, P_i, and a constant applied displacement, δ_i. For the constant force case and a crack arrest position α this energy is

$$\Delta U_P = P_i[\delta(\alpha) - \delta(\alpha_0)] = P_i^2 \frac{C_V(\alpha) - C_V(\alpha_0)}{E'B}. \tag{1(a)}$$

The values $\delta(\alpha)$ and $\delta(\alpha_0)$ are the load-line displacements at arrest and formation, respectively. For a constant displacement the excess elastic energy becomes

$$\Delta U_\delta = \delta_i[P(\alpha_0) - P(\alpha)] = \delta_i^2 E'B\left[\frac{1}{C_V(\alpha_0)} - \frac{1}{C_V(\alpha)}\right], \tag{1(b)}$$

where $P(\alpha_0)$ and $P(\alpha)$ are the resulting forces at crack formation and arrest. The chevron compliance values $C_V(\alpha_0)$ and $C_V(\alpha)$ in equations (1(a)) and (b) are dimensionless, $C_V = \delta(\alpha)E'B/P(\alpha)$, where E' is the elastic modulus.

The constant formation force, P_i, or formation displacement, δ_i, necessary to produce a sharp crack depends on machine notch bluntness, ρ, and the dimensions for W, B, α_0 and α_1. Therefore one is left with the issue of establishing a crack formation criterion which is independent of these factors so that any comparison between two or more selected chevron geometries is equitable. Recognizing that overloading occurs because of a blunt prenotch, a criterion can be established as shown in figure 3 using an equivalent crack tip threshold stress level, σ_{cr}. The stress in the vicinity of a blunt crack with a radius ρ is approximated as (ref. 7)

$$\frac{\sigma_{cr}\sqrt{\pi\rho}}{2} = K_f(\alpha_0) \tag{2}$$

where the value $K_f(\alpha_0)$ is the chevron tip stress singularity. Using an approach based on the slice model concept of Bluhm (ref. 1), the stress singularity for a finite slice of material B' wide (and a resolved straight crack front) in the center of the chevron section is written as

$$K_f(\alpha_0) = \frac{Y_s(\alpha_0)P_i'(S_1 - S_2)}{WB'\sqrt{W}}. \tag{3}$$

In this expression $Y_s(\alpha_0)$ is a dimensionless boundary correction term for a straight-through crack of length α_0 and P_i' is the strip force. The term $Y_s(\alpha_0)$ for a straight-through cracked beam subjected to four-point bending is taken from Srawley and Gross (ref. 6) as

5

$$Y_s(\alpha) = \frac{3\sqrt{\alpha}}{(1-\alpha)^{3/2}}\left[1.9887 - 1.326\alpha - \frac{(3.49 - 0.68\alpha + 1.35\alpha^2)\alpha(1-\alpha)}{(1+\alpha)^2}\right].$$ (4)

The strip force, P_i', is related to the formation displacement, δ_i, and the dimensionless straight-through cracked compliance, $C_s(\alpha_0)$, such that

$$P_i' = \frac{E'k\delta_i B'}{C_s(\alpha_0)} = \frac{K_f(\alpha_0)WB'\sqrt{W}}{Y_s(\alpha_0)(S_1 - S_2)}.$$ (5)

Recognizing that the strip is only part of the whole, a shear factor 'k' is introduced to account for the interlaminar compatibility.

The relationship between σ_{cr} and $K_f(\alpha_0)$ given in equation (2) is now used with equation (5) to produce a formation displacement expression

$$\delta_i = \frac{\sigma_{cr}\sqrt{\pi\rho}}{2}\frac{W\sqrt{W}}{Y_s(\alpha_0)(S_1 - S_2)}\frac{C_s(\alpha_0)}{kE'}.$$ (6)

The full beam compliance relates the formation force and displacement such that

$$P_i = \frac{\sigma_{cr}\sqrt{\pi\rho}}{2}\frac{WB\sqrt{W}}{Y_s(\alpha_0)(S_1 - S_2)}\frac{C_s(\alpha_0)}{kC_f(\alpha_0)}.$$ (7)

The formation force expression, when substituted into equation (1(a)) for the constant force excess elastic energy, provides

$$\Delta U_P = \frac{\sigma_{cr}^2 \pi\rho}{4E'}\frac{W^3B[C_f(\alpha) - c_f(\alpha_0)]}{Y_s^2(\alpha_0)(S_1 - S_2)^2}\left[\frac{C_s(\alpha_0)}{kC_f(\alpha_0)}\right]^2.$$ (8(a))

Similarly, combining equation (6) with the constant displacement expression for excess energy, equation (1(b)), yields the expression

$$\Delta U_\delta = \frac{\sigma_{cr}^2 \pi\rho}{4E'}\frac{W^3B}{Y_s^2(\alpha_0)(S_1 - S_2)^2}\left[\frac{C_s(\alpha_0)}{k}\right]^2\left[\frac{1}{C_f(\alpha_0)} - \frac{1}{C_f(\alpha)}\right].$$ (8(b))

Equations (8(a)) and (b) express the driving energy released between formation and subsequent arrest within the stable region. The energy resisting propagation must be accounted for in developing the overload resistance factors for the constant applied force and displacement cases. The resistive energy is the same for both a constant force and a constant displacement. For flat R-curve materials, it is simply the critical fracture toughness measure, G_{IC}, multiplied by half of the newly created fracture area after arrest, or

$$\Delta\Omega = G_{Ic} \cdot A = \frac{K_{Ic}^2}{E'} \frac{WB}{2} \frac{(\alpha - \alpha_0)^2}{(\alpha_1 - \alpha_0)} \qquad (9)$$

Defined as the ratio of resistance energy to driving energy, $\Delta\Omega/\Delta U$, the overload resistance factor for a constant applied force becomes[3]

$$S_P = \frac{2K_{Ic}^2}{\sigma_{cr}^2 \pi \rho} \frac{Y_S^2(\alpha_0)(S_1 - S_2)^2}{W^2[C_V(\alpha) - C_V(\alpha_0)]} \left[\frac{kC_V(\alpha_0)}{C_S(\alpha_0)}\right]^2 \left.\frac{(\alpha - \alpha_0)^2}{\alpha_1 - \alpha_0}\right|_{\alpha < \alpha_{min}} , \qquad (10(b))$$

and for the constant applied displacement is

$$S_\delta = \frac{2K_{Ic}^2}{\sigma_{cr}^2 \pi \rho} \frac{Y_S^2(\alpha_0)(S_1 - S_2)^2 k^2}{W^2 C_S^2(\alpha_0)} \left[\frac{C_V(\alpha_0)C_V(\alpha)}{C_V(\alpha) - C_V(\alpha_0)}\right] \left.\frac{(\alpha - \alpha_0)^2}{\alpha_1 - \alpha_0}\right|_{\alpha < \alpha_{min}} \qquad (10(a))$$

In the comparative analysis of selected chevron geometries it is assumed that beams have the same notch acuity and material properties. The first term on the right in both equations (10(a)) and (b) can be neglected and set to unity. A valid chevron-notch specimen test requires stability prior to instability. Accordingly, the crack arrest position, α, used to evaluate the overload resistance factor is selected such that $\alpha < \alpha_{min}$. The overload resistance evaluation can be made once the chevron compliance values $C_V(\alpha_0)$ and $C_V(\alpha)$ are known.

COMPLIANCE ANALYSIS

The compliance of a chevron-notched beam can be obtained experimentally (ref. 3) or estimated analytically. A suitable parametric study can be accomplished analytically using Bluhm's slice model method. Bluhm imagined the cross-section of a chevron to be constructed of slices as shown in figures 4(a) and (b). After accounting for displacement compatibility between slices with a shear factor, k, the total chevron compliance is estimated as the sum of the slice compliances. The beam compliance formulation for a straight-through crack, $C_S(\alpha)$, is used to evaluate the compliance of each slice. The algorithm or estimating the chevron compliance having a relative crack length, α, is

---

[3]The symbols S_P and S_δ should not be confused with S_1 and S_2 used to represent the major and minor loading spans. Although different nomenclature may have been chosen for the overload resistance factor, these symbols were taken from Bluhm (ref. 2) for consistency.

$$\frac{1}{C_V(\alpha_i)} = \frac{1}{n}\left(\frac{i}{C_S(\alpha_i)} + k\sum_{j=i+1}^{n}\frac{1}{C_S(\alpha_j)}\right), \tag{11}$$

where n is the number slices through a cross-section. To insure that compliance estimations are not dependent on slice thickness, the number of slices in this study is $n=400$. The shear correction term, k, accounting for interlaminar compatibility in both the overload force and chevron compliance estimations is taken from Bluhm (ref. 1). Bluhm compared experimental compliance measurements to slice model predictions and developed the following relationship for the shear correction term

$$k = \left|\begin{array}{ll} 1+\alpha_1^{3.12}(2.263\theta-4.744\theta^2+4.699\theta^3-1.774\theta^4) & 0<\theta<1 \\[2em] 1+0.444\alpha_1^{3.12} & \theta>1 \end{array}\right. \tag{12}$$

where θ is the angle of the base of the chevron measured in radians. It can be seen that k depends on the chevron base angle, θ, and base position, α_1. The straight-trough beam compliance is calculated using $Y_S(\alpha)$ in equation (4) based on the technique outline by Munz, Bubsey, and Shannon (ref. 5).

A potentially large selection of chevron notched geometries can be examined, and a rational analytical approach which clearly identifies the influence of each geometric dimension must be established. The approach here first examines how various α_0 influence the specimen response for selected constant values of $\alpha_1-\alpha_0$. A second effort then examines how the difference $\alpha_1-\alpha_0$ influences the same fracture response for selected constant values of α_0. The fracture response parameters of interest are the critical crack length, the critical crack front length, and the fracture area included in the stable region. These parameters are plotted versus the overload resistance factor. It is unlikely that each response reaches its optimized value for the same geometry, therefore one may need to balance each response to obtain an optimum specimen design. Defining exactly what constitutes a 'good balance' between crack length, crack front length, and premature failure resistance may depend on the experimentalist's interests.

DISCUSSION

Compliance

One conclusion from the parametric study is that the chevron-notch specimen performance is insensitive to the width to thickness ratio, W:B. Provided values for α_0 and α_1 were constant, values for α_{min}, $Y_V(\alpha_{min})$, and S_p were independent of W:B. This result was expected since it relates directly to the properties of elastic similitude. As an explanation, consider the chevron geometries in figures 4(a) and (b) which are divided into an equal number of slices. It is obvious that slices in

8

figure 4(a) having the same average crack length as those in figure 4(b) will also have essentially the same dimensionless compliance. Any difference relates to changes in the base angle, θ, and the associated small changes in the shear correction term, k. Since the total compliance for each geometry is the sum of the slice compliances, both geometries have nearly identical dimensionless compliances. The small compliance differences due to changes in the shear correction factor are further minimized when the compliance slope is examined, and it is the compliance slope that affects the fracture response.

Changes in the dimensionless crack area with crack length, α, are also the same for both geometries, therefore the dimensionless energy release rate, stress intensity factor, critical crack length and overload resistance factors are essentially independent of W:B. Since the fracture response of a beam is insensitive to W:B a fixed ratio of W:B=2:1 is used in what follows. Comparisons are made in relation to fixed values of $\alpha_1 - \alpha_0$ for varying α_0 positions, and fixed α_0 values with varying $\alpha_1 - \alpha_0$ values. The support span, S_1, is set at four times the width of the bend beam, and the loading span, S_2, is half the size of the support distance. A Poisson's ratio of $v = 0.285$ is assumed in this study to calculate the un-notched beam compliance.

Stress Intensity Factors

Figure 5(a) is a plot of stress intensity as a function of the dimensionless crack extension, $(\alpha - \alpha_0)$, for $\alpha_0 = 0.2$ and three values of $\alpha_1 = 1.0, 0.8, 0.6$. The trend for both α_{min} and $Y_V(\alpha_{min})$ is typical for changes in $\alpha_1 - \alpha_0$. Figure 5(a) shows that increasing α_1 for constant values of α_0 increases the overall length of the stable region. Increasing α_1 also produces higher $Y_V(\alpha)$ values which decline more gradually to $Y_V(\alpha_{min})$. It is the slope of $Y_V(\alpha)$ which dictates how much energy is available to sustain propagation after formation. A more gradually sloped $Y_V(\alpha)$ implies higher driving energies for crack extension which is the case for large α_1 values. However, the actual energy available will depend on the magnitude of the overload force, which will be less for large α_1 since values of $Y_V(\alpha)$ are also large. Thus, the slope of $dK(\alpha)/d\alpha$ does not completely characterize the tendency for a beam to fail prematurely. The variation in $Y_V(\alpha)$ for $\alpha_1 - \alpha_0 = 0.50$ and relative tip positions $\alpha_0 = 0.20, 0.30, 0.40,$ and 0.50 is shown in figure 5(b). It is seen that positioning the chevron tip deep into a specimen has some undesirable effects. Large α_0 values produce both smaller crack extension increments, $\Delta\alpha_{min}$, and crack front lengths, β_{min}, at instability because of the strong influence of the specimen back face. Smaller $\Delta\alpha_{min}$ values reduces the crack area in the stable region and, consequently, the resistive energy in the overload factor evaluation. Large α_0 positions also generate high $Y_V(\alpha)$ values with more gradual slopes before $Y_V(\alpha_{min})$, which means more energy is available to sustain crack extension after formation.

Although little attention has been given to $Y_V(\alpha)$ values after the instability point, it can be imagined that they influence fracture measurements for rising R-curve materials. For these materials the higher elastic energy supply rates beyond α_{min} may be needed to offset inherent material resistance increases to produce instability. It is seen in figure 5(b) that smaller α_0 positions produce a flatter response in the $Y_V(\alpha)$ curve after $Y_V(\alpha_{min})$. A flatter curve could be more desirable for rising R-curve materials since the more gradual increase may prolong stable extension such that a peak material resistance is realized. Even if the interplay between the $Y_V(\alpha)$ curve and material resistance is neglected, $Y_V(\alpha)$ values surrounding α_{min} for a flat curve are less sensitive to crack length changes from stability to instability. In theory, the shape of $Y_V(\alpha)$ does not affect fracture measurements for materials with flat R-curve behavior. Nearly any configuration produces a valid fracture toughness

measurement provided a sharp crack has been successfully initiated. However, the overload resistance factor places additional limits on a specimen's design which also must be considered.

Overload Resistance Factor

Analysis of the overload resistance of chevron beams subjected to four-point bending reveals essentially the same trends whether fixed displacement or fixed force conditions are applied to the boundary. The fixed displacement overload resistance, S_δ, is always larger than the fixed force, S_P, for the same chevron configuration. This is expected since there is no energy input for the fixed displacement case and the amount of free energy available for crack propagation is limited. For a constant applied force, work is done on the specimen during crack extension making it a more severe case in terms of fracture stability. The amount of work done is related directly to the formation force and change in compliance with crack extension, $P_i^2[C_\gamma(\alpha)-C_\gamma(\alpha_0)]$. Since similar trends are observed for both S_δ and S_P, and the fixed force case is considered to be more severe, only the results for fixed force conditions are considered in this discussion. Moreover, constant applied forces are likely to be more prevalent experimentally such that S_P may also be more meaningful[4].

The crack arrest position after formation, α, selected for this study divides the chevron's crack area within the stable region in half. Although the selection is arbitrary, a crack area measure relates linearly with the resistive energy used in the overload formulation and provides an equivalent comparison for each selected geometry. Obviously both the resistive energy and the driving energy depend on the selected arrest position. Fortunately the ratio $S_P=\Delta U/(\gamma\Delta A)$ is not greatly affected by α, and comparative results for various chevron geometries are even less affected provided the crack area measures are constant. In the remaining discussion, resistance factors are examined in relation to the dimensionless critical crack length, α_{min}, critical crack width, β_{min}, and total crack area, $\beta_{min}\Delta\alpha_{min}$.

Selected α_1-α_0 with varying α_0

Changes in $\Delta\alpha_{min}$ for constant values of α_1-α_0 and various α_0 positions are shown in figure 6. In general large α_1-α_0 values produce large amounts of crack extension. The largest amount of crack extension occurs for α_1-α_0=0.8 with $\alpha_0\leq0.15$, where $\Delta\alpha_{min}$ is extends to nearly twenty percent of the beam depth. Large α_1-α_0 values also produce small overload resistance factors. These low factors suggests that a higher premature failure frequency will accompany geometries having the largest stable region lengths. Figure 6 shows that higher S_P values can be obtained for smaller differences in α_1-α_0 provided the chevron tip is positioned slightly deeper in the beam. However, the stable region length is also reduced for small α_1-α_0 values positioned deep into the beam. The smallest α_1-α_0 values produce the best overload resistance factors but resulting crack extension values may be too small. Geometries with $\Delta\alpha_{min}$ less then ten times the prenotch radius may produce measurements which are influenced by machine notch bluntness. This imposes a practical limit which must be considered for smaller α_1-α_0 values. Improved overload resistance factors can be achieved without significant loss in crack extension length for geometries with α_0=0.2, α_1=0.8 or α_0=0.25, α_1=0.75.

---

[4]Even for fixed displacement control, deformations between contact points in the load train are capable of sustaining nearly constant force levels during sudden crack extension. This is particularly true for very stiff materials such as ceramics where achieving fixed displacement conditions at the specimen interface may be impossible (ref. 4).

The effects of $\alpha_1-\alpha_0$ on the critical crack front length are displayed in figure 7. It is seen that both β_{min} and the overload resistance factor increase for smaller $\alpha_1-\alpha_0$ values. Examining one curve for a selected constant value of $\alpha_1-\alpha_0$ shows that large α_0 positions tend to maximize the dimensionless crack front length. However, β_{min} values drop off for even larger α_0 positions because of the specimen back face influence is strong. Peak β_{min} values are obtained for the cases $\alpha_1-\alpha_0=0.60$ with $\alpha_0=0.20$, and $\alpha_1-\alpha_0=0.50$ with $\alpha_0=0.25$. Although $\alpha_1-\alpha_0=0.3$ produces the largest crack front length, the crack extension increment is likely too small to provide accurate measurements. The crack area $\beta_{min}\Delta\alpha_{min}$ is shown in figure 8. Only modest losses in the crack area result for improved overload resistance performance. Examining figures 6, 7 and 8 shows that, provided α_0 is move deeper into the beam, there is benefit in selecting reduced $\alpha_1-\alpha_0$ values for testing.

Selected α_0 with varying $\alpha_1-\alpha_0$

The relationship between the overload resistance factor and critical crack length for constant α_0 and varying $\alpha_1-\alpha_0$ is given in figure 9. The overload resistance factor increases and the crack extension increment decreases the smaller $\alpha_1-\alpha_0$ is for each selected α_0 value. Maximum crack growth occurs for $\alpha_1=1.0$ where the chevron extends fully through the cross section for each selected α_0. Reducing α_1 reduces the crack extension length but the added benefit is an increase in the overload resistance. The crack front length versus overload resistance factor relationship in figure 10 show larger β_{min} values and overload resistances with smaller $\alpha_1-\alpha_0$ for each α_0 value. What remains unclear after examining figure 9 and figure 10 is which position for α_0 produces the best balance between the loss in crack extension and the gain in crack front length and overload resistance. However, a significant improvement in β_{min} and S_p occur for α_0 positions of 0.2 and 0.3 compared to $\alpha_0=0.10$ with a limited loss in $\Delta\alpha_{min}$. Although additional improvement in the crack front length and overload resistance is observed for $\alpha_0=0.40$ and $\alpha_0=0.50$, this improvement does not offset the additional loss in the crack extension increment.

Since the crack length decreases and the front length increases with smaller $\alpha_1-\alpha_0$ for each α_0 selected, the critical crack area peaks in figure 11 are expected. The largest stable region crack area occurs for $\alpha_0=0.10$ and $\alpha_1=0.90$ but the overload resistance for this geometry is low. The large improvements in the overload resistance observed for $\alpha_0=0.20$ and $\alpha_0=0.30$ can be obtained with little loss in crack area provided α_1 is not extended to the full beam depth. The crack area peaks at $\alpha_1 \leq 1.0$ for both $\alpha_0=0.20$ and $\alpha_0=0.3$. Once again the additional gains in S_p realized for $\alpha_0 > 0.30$ may not offset the loss in $\Delta\alpha_{min}$. A balance among the overload resistance, the critical crack length, and critical crack front length is expected for chevron geometries with $\alpha_0=0.20$, $\alpha_1=0.70$ and $\alpha_0=0.30$, $\alpha_1=0.80$. As seen in figure 11, α_1 values slightly less than 1.0 generate gains in the crack area within the stable region.

The fixed-force and fixed-displacement overload resistance formulations proposed here are physically based comparisons between the excess energy required to initiate a sharp crack and the fracture energy available for arrest within the subcritical region of a chevron geometry. The driving energy is related to changes in compliance with crack extension and the arresting energy is proportional to the crack area. In formulating the overload resistance, a smaller crack area implies a lower S_p factor, however these factors actually increase even though crack area decreases. The physical explanation for this apparent contradiction rests with comparative differences in compliance before formation and after arrest, and it is here that the chevron base position influence is understood. Selecting a small value for α_1 will yield smaller changes in compliance which minimize the energy sustaining propagation. Conversely, large α_1 values produce large compliance changes with crack extension and subsequently larger amounts of free elastic energy.

A chevron's tip position, α_0, affects the overload resistance somewhat differently, as it determines the force required to form a sharp crack. Large α_0 positions generate a low formation force which reduce the driving energy for extension. Small $\alpha_1 - \alpha_0$ values produce more rapid gains in crack area with crack extension which imposes a high resistance energy as the crack extends after formation. This has a positive effect on the overload resistance factor. Optimizing the overload resistance factor tends to minimize $\alpha_1 - \alpha_0$ and push α_0 deeper into the beam. There are additional gains in the critical crack front length. However, the $\alpha_1 - \alpha_0$ value has a lower limit since it must be large enough to produce the crack extension increments necessary for accurate fracture toughness measurements. Crack extension also controls how large α_0 can be, because a strong influence from the specimen back face reduces the stable region size. A summary of the fracture parameters for the recommended range of geometries is shown in table I. The critical dimensionless stress intensity factor increases with increasing α_1 and α_0 values.

As a final note it is worth commenting that selected values for the support and loading spans influence the overload resistance in terms of the test setup. In general, a smaller difference between the support and loading spans and a reduced size for the loading span will improve the overload resistance for any chevron configuration. This essentially translates to limiting the amount of stressed material and therefore the stored energy. This trend is expected and it is consistent with the improved crack formation performance of three-point loading compared to four-point loading.

CONCLUSIONS

1. Dimensionless beam compliance, critical crack length, critical crack front length and stress intensity are essentially independent of the W:B ratio.

2. Physically based overload resistance formulations are developed for fixed-displacement and fixed force conditions. These formulations disclose additional considerations which may bound the selection of chevron configurations for standardized testing.

3. The tip position of the chevron, α_0, primarily affects the force level required to initiate a sharp crack. Although a shallow position for α_0 maximizes crack growth, deeper positions produce lower formation forces which will improve the chance of arrest after crack formation.

4. The base position of the chevron affects beam compliance changes after formation. The critical crack length, $\Delta\alpha_{min}$, is maximized for large α_1 positions, however, improved overload resistances are obtained if the base position does not extend the full beam depth.

5. The selection of chevron geometries having a good balance of overload resistance, critical crack length, and the critical crack front length is narrow. Based on this study, this balance can be achieved for chevron geometries with $0.20 \leq \alpha_0 \leq 0.30$ and $0.70 \leq \alpha_1 \leq 0.80$.

REFERENCES

1. Bluhm, J.I.: Slice Synthesis of a Three Dimensional 'Work of Fracture' Specimen - for Brittle Materials Testing." Eng. Fract. Mech., vol. 7, Sept. 1975 pp. 593–604.

2. Bluhm, J.I.: Stability Considerations in a Generalized Three Dimensional 'Work of Fracture' Specimen. Fracture vol. 3, D.M.R. Taplin, ed., University of Waterloo press, Waterloo, Ontario, Canada, 1977, pp. 409–417.

3. Calomino, A.M.; Bubsey, R.; and Ghosn, L.: Compliance Measurements of the Chevron Notched Four-point Bend Specimen." NASA TM–106538, 1994.

4. Calomino, A.M.; Brewer, D.N.: Controlled Crack Growth Specimen for Brittle Systems. J. Am. Ceram. Soc., vol. 75, no. 1, 1992, pp. 206–208.

5. Munz, D.; Bubsey, R.T.; and Shannon, J.: Fracture Toughness Determination of Al_2O_3 Using Four Point Bend Specimens with Straight-Through and Chevron Notches. J. Am. Ceram. Soc., vol. 63, no. 5–6, 1980, pp. 300–305

6. Srawley, J.E.; and Gross, B.: Side-Cracked Plates Subject to Combined Direct and Bending Forces. Cracks and Fracture: Proceedings of the Ninth National Symposium on Fracture Mechanics, ASTM STP601, American Society for Testing and Materials, Philadephia, PA, 1976, pp. 559–70.

7. Tada, H.; Paris, P.C.; and Irwin, G.R.: **The Stress Analysis of Cracks Handbook**, second ed., Del Research Corporation, St. Louis, MO, 1985, 1.7–1.9.

8. Wu, S.X.: Stability and Optimum Geometry of Chevron Notched Three-Point Bend Specimens. Int. J. Frac., vol. 26, no. 2, 1984, R43-47.

TABLE I.—DIMENSIONLESS CHEVRON NOTCH
STRESS INTENSITY FACTOR AND SUB-
CRITICAL CRACK GROWTH INCREMENT,
CRACK WIDTH, AND CRACK AREA FOR
THE RECOMMENDED RANGE OF
CHEVRON GEOMETRIES.

α_0	α_1	$Y_v(\alpha_{min})$	$\Delta\alpha_{min}$	β_{min}	$\beta_{min}\,\Delta$
	0.70	5.66	0.145	0.290	0.0420
0.20	0.75	6.13	0.155	0.282	0.0439
	0.80	6.59	0.163	0.272	0.0446
	0.70	6.14	0.138	0.307	0.0425
0.25	0.75	6.66	0.147	0.295	0.0435
	0.80	7.23	0.155	0.282	0.0439
	0.70	6.65	0.129	0.322	0.0416
0.30	0.75	7.25	0.141	0.312	0.0439
	0.80	7.90	0.146	0.292	0.0428
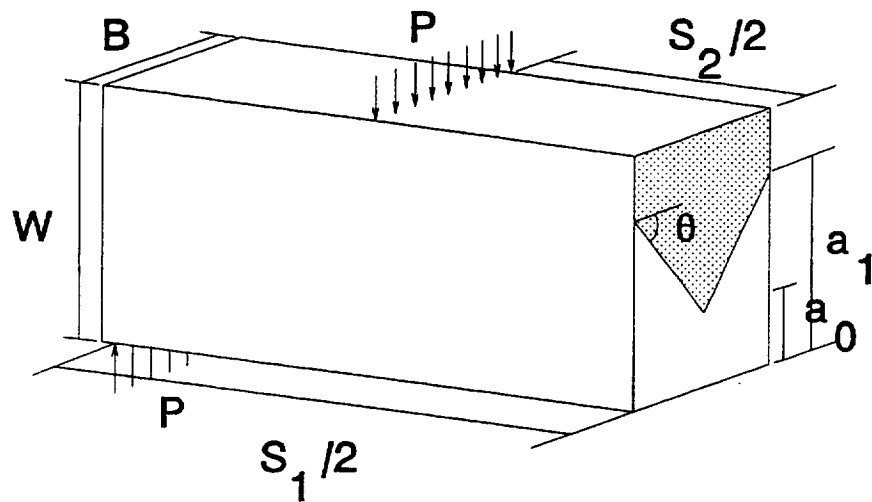
Figure 1.—Geometry of a chevron-notched four-point bend specimen (one half of specimen shown).
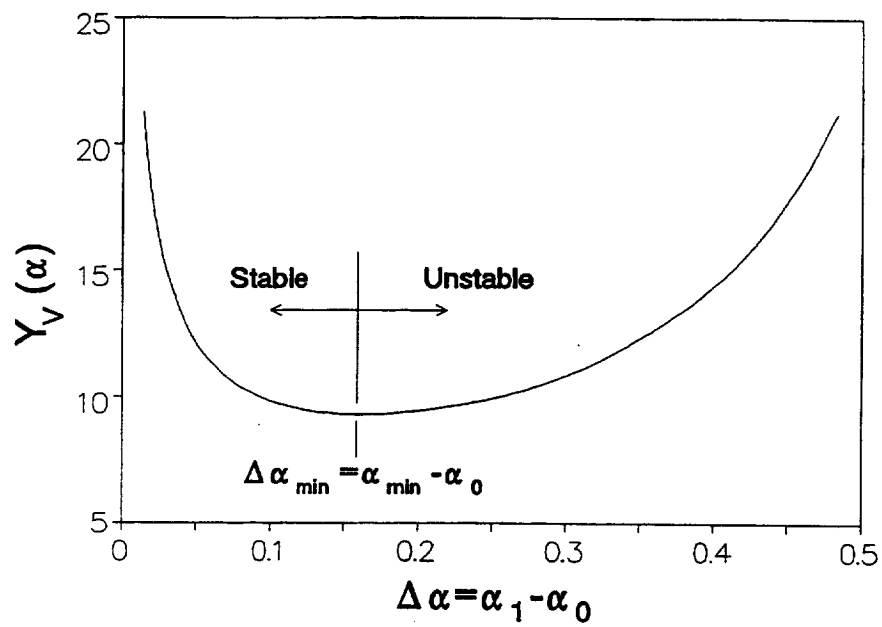
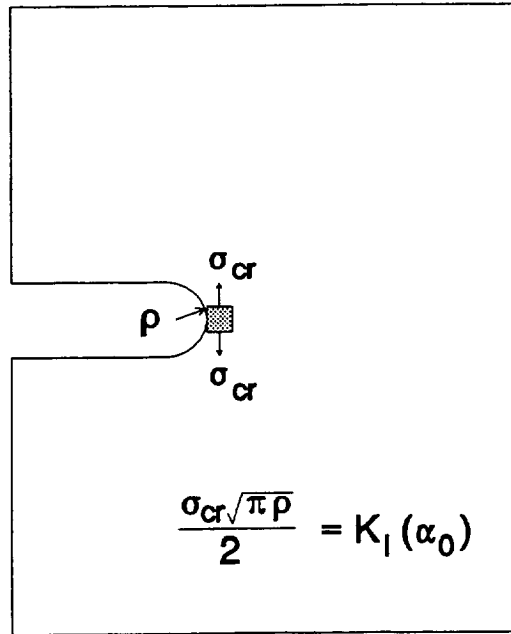Figure 2.—Typical dimensionless stress intensity for a chevron-notch bend specimen.

14

$$\frac{\sigma_{cr}\sqrt{\pi\rho}}{2} = K_I(\alpha_0)$$

Figure 3.—Crack-tip stress for a blunt notch with radius ρ. The value σ_{cr} is used as the criterion for crack formation.
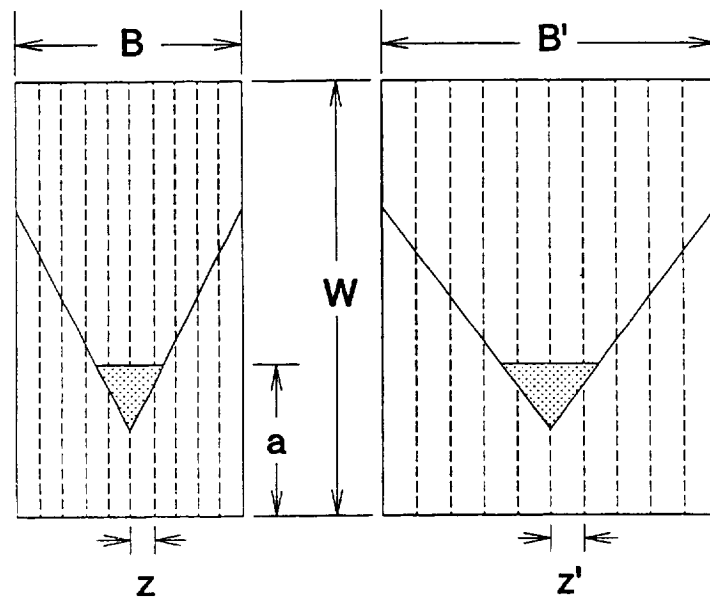

Figure 4.—Bluhm slice model concept for estimating beam compliance. Width to thickness ratio, W:B, has little affect on nondimensional compliance when α_0 and α_1 are equal.
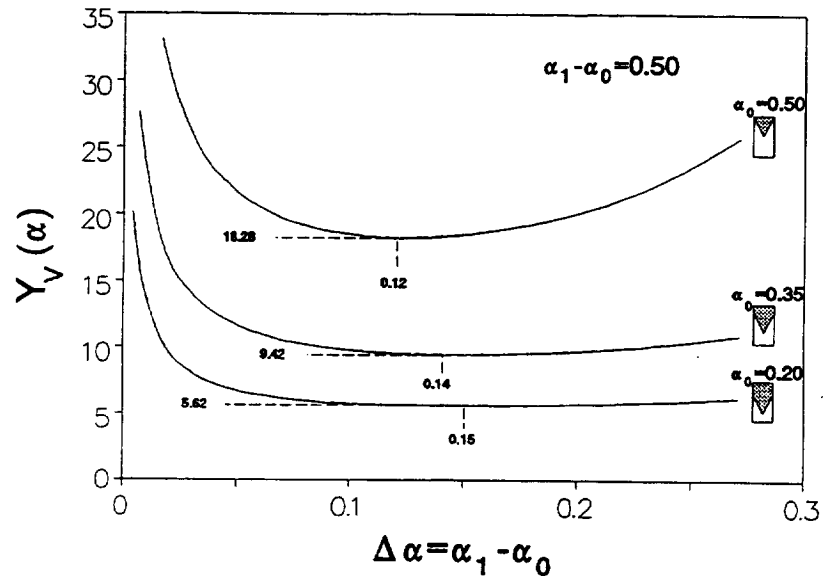
Figure 5(a).—Dimensionless stress intensity for $\alpha_1 - \alpha_0 = 0.5$ and selected α_0 values showing the potential increase in excess energy for large α_0 values.
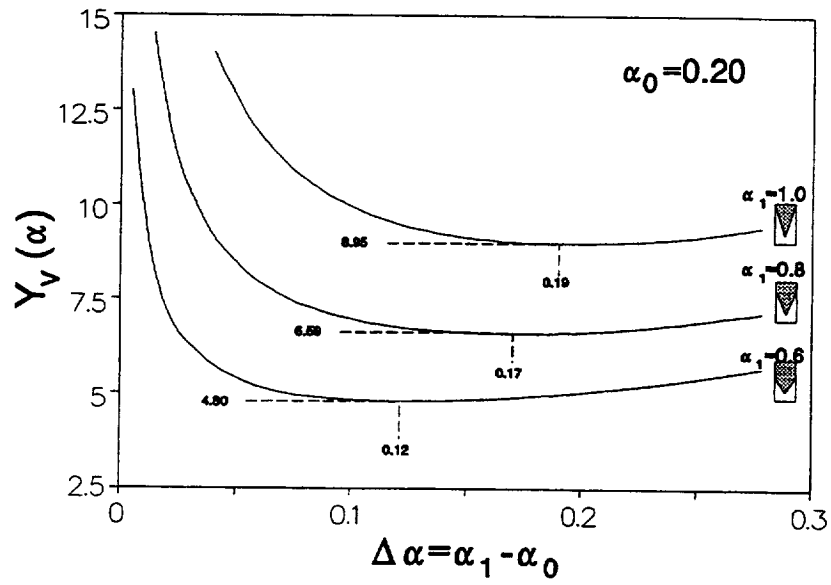
Figure 5(b).—Dimensionless stress intensity for $\alpha_0 = 0.2$ and selected α_1 values showing the potential increase in excess energy for large α_1 values.
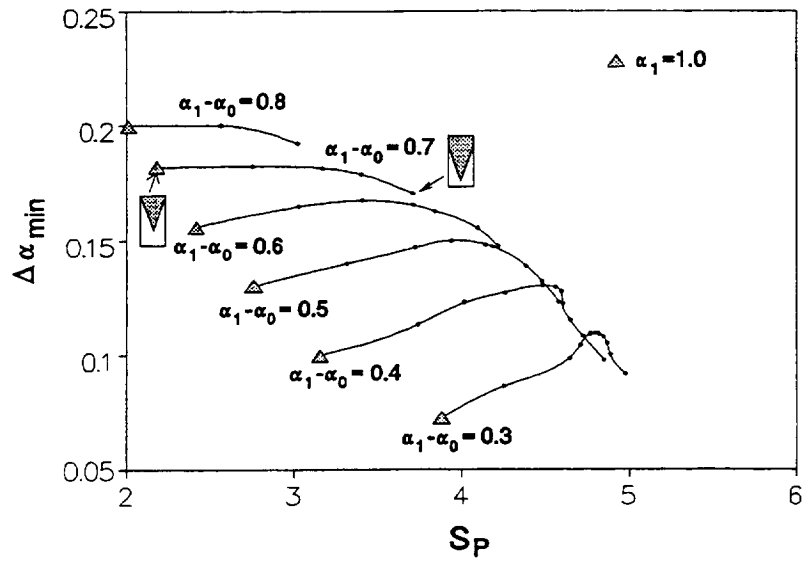
Figure 6.—Crack extension vs overload resistance for selected $\alpha_1\text{-}\alpha_0$ values. Points represent 0.05 increment changes in α_0, right to left, up to a $\alpha_1 = 1.0$ limit.
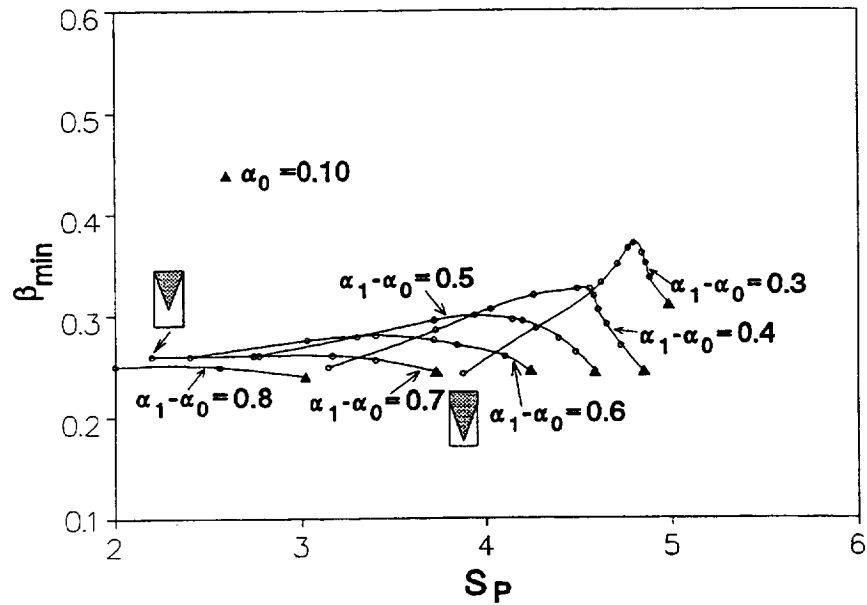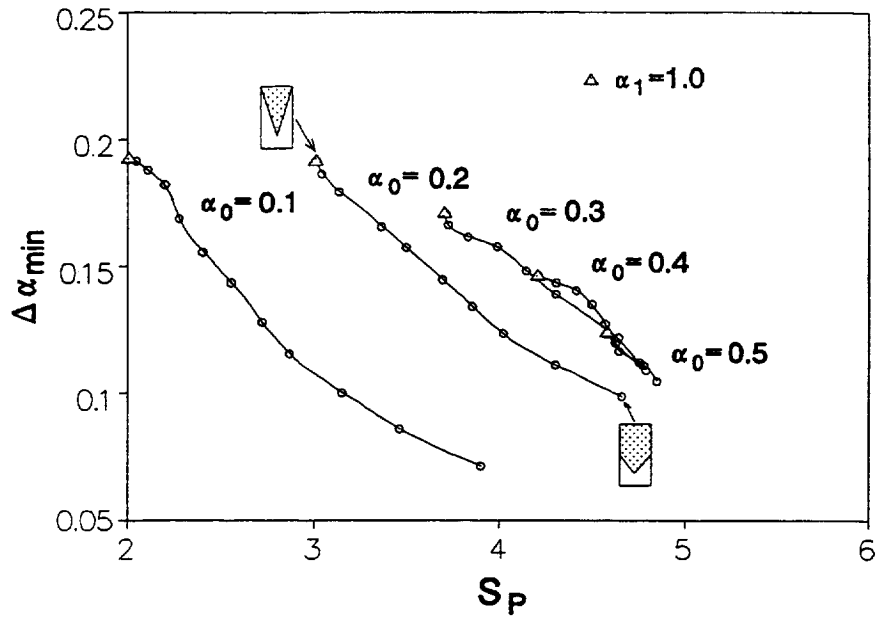

Figure 7.—Crack width vs overload resistance for selected $\alpha_1\text{-}\alpha_0$ values. Points represent 0.05 incremental changes in α_0, right to left, up to a $\alpha_1 = 1.0$ limit.
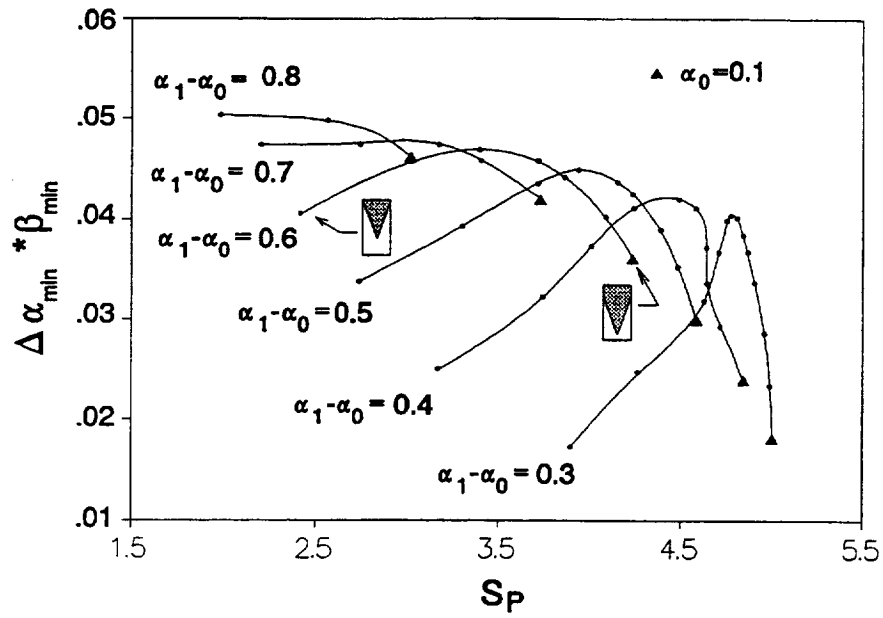
Figure 8.—Crack area vs overload resistance for selected α_1-α_0 values. Points represent 0.05 incremental changes in α_0, right to left, up to α_1 = 1.0 limit.

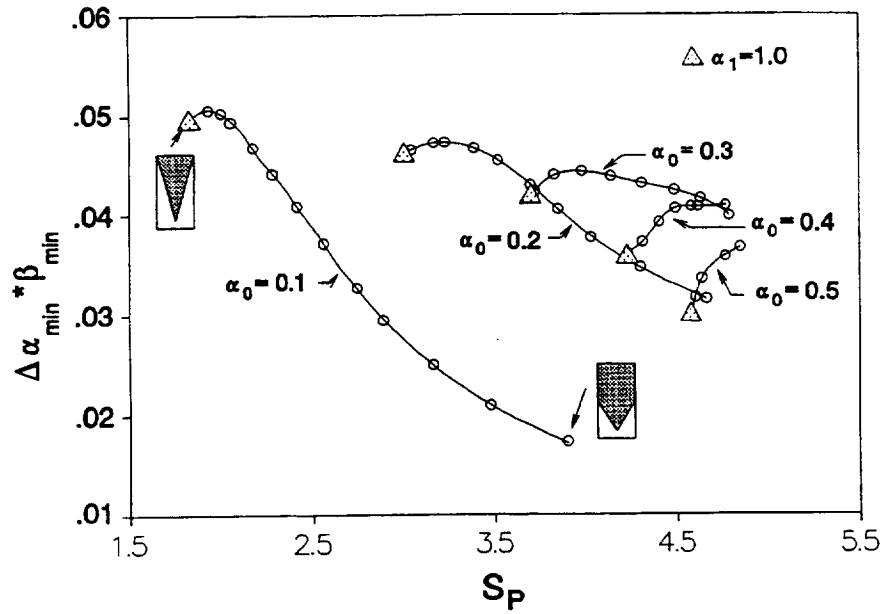
Figure 9.—Crack extension vs overload resistance for selected α_0. Points represent 0.05 changes in α_1, left to right, from α_1 = 1.0 to α_1-α_0 = 0.30.

18
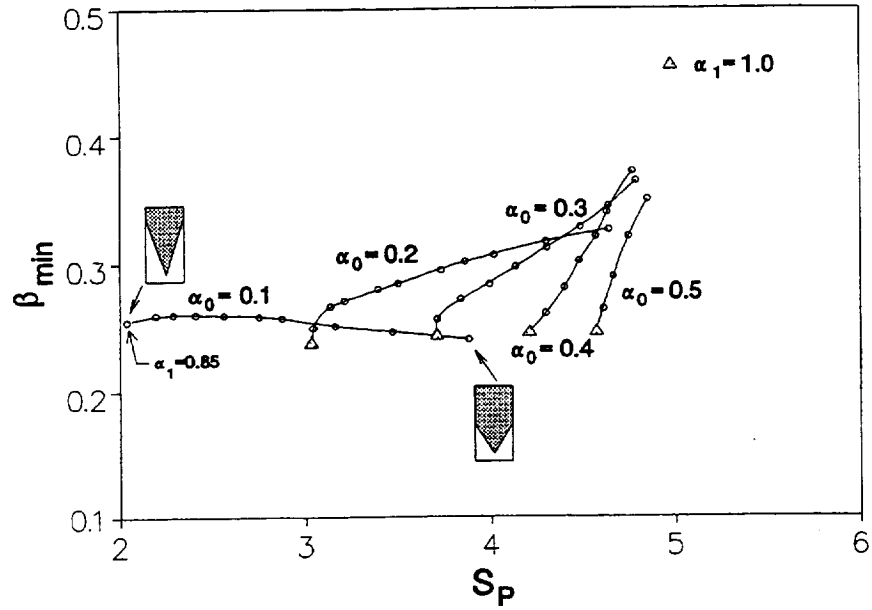
Figure 10.—Crack width vs overload resistance for selected α_0 values. Points on each curve are 0.05 changes in α_1, left to right, from $\alpha_1 = 1.0$ to $\alpha_1-\alpha_0 = 0.30$.

Figure 11.—Crack extension vs overload resistance for selected α_0 values. Points on each curve are 0.05 changes in α_1, left to right, from $\alpha_1 = 1.0$ to $\alpha_1-\alpha_0 = 0.30$.

19

REPORT DOCUMENTATION PAGE

Public reporting burden for this collection of information is estimated to average 1 hour per response, including the time for reviewing instructions, searching existing data sources, gathering and maintaining the data needed, and completing and reviewing the collection of information. Send comments regarding this burden estimate or any other aspect of this collection of information, including suggestions for reducing this burden, to Washington Headquarters Services, Directorate for Information Operations and Reports, 1215 Jefferson Davis Highway, Suite 1204, Arlington, VA 22202-4302, and to the Office of Management and Budget, Paperwork Reduction Project (0704-0188), Washington, DC 20503.

1. AGENCY USE ONLY (Leave blank)	2. REPORT DATE	3. REPORT TYPE AND DATES COVERED
	August 1994	Technical Memorandum

4. TITLE AND SUBTITLE

The Role of Crack Formation in Chevron-Notched Four-Point Bend Specimens

5. FUNDING NUMBERS

WU–505–63–52

6. AUTHOR(S)

Anthony M. Calomino and Louis J. Ghosn

7. PERFORMING ORGANIZATION NAME(S) AND ADDRESS(ES)

National Aeronautics and Space Administration
Lewis Research Center
Cleveland, Ohio 44135–3191

8. PERFORMING ORGANIZATION REPORT NUMBER

E–8948

9. SPONSORING/MONITORING AGENCY NAME(S) AND ADDRESS(ES)

National Aeronautics and Space Administration
Washington, D.C. 20546–0001

10. SPONSORING/MONITORING AGENCY REPORT NUMBER

NASA TM–106631

11. SUPPLEMENTARY NOTES

12a. DISTRIBUTION/AVAILABILITY STATEMENT

Unclassified - Unlimited
Subject Category 39

12b. DISTRIBUTION CODE

13. ABSTRACT (Maximum 200 words)

The failure sequence following crack formation in a chevron-notched four-point bend 1 specimen is examined in a parametric study using the Bluhm slice synthesis model. Premature failure resulting from crack formation forces which exceed those required to propagate a crack beyond α_{min} is examined together with the critical crack length and critical crack front length. An energy based approach is used to establish factors which forecast the tendency of such premature failure due to crack formation for any selected chevron-notched geometry. A comparative study reveals that, for constant values of α_1 and α_0, the dimensionless beam compliance and stress intensity factor are essentially independent of specimen width and thickness. The chevron tip position, α_0, has its primary effect on the force required to initiate a sharp crack. Small values for α_0 maximize the stable region length, however, the premature failure tendency is also high for smaller α_0 values. Improvements in premature failure resistance can be realized for larger values of α_0 with only a minor reduction in the stable region length. The stable region length is also maximized for larger chevron based positions, α_1, but the chance for premature failure is also raised. Smaller base positions improve the premature failure resistance with only minor decreases in the stable region length. Chevron geometries having a good balance of premature failure resistance, stable region length, and crack front length are $0.20 \leq \alpha_0 \leq 0.30$ and $0.70 \leq \alpha_1 \leq 0.80$.

14. SUBJECT TERMS

Chevron-notch, Four point bend; Overload resistance factor; Crack stability; Subcritical crack length

15. NUMBER OF PAGES

21

16. PRICE CODE

A03

17. SECURITY CLASSIFICATION OF REPORT	18. SECURITY CLASSIFICATION OF THIS PAGE	19. SECURITY CLASSIFICATION OF ABSTRACT	20. LIMITATION OF ABSTRACT
Unclassified	Unclassified	Unclassified	